Exploitation of Acoustic Noise Correlation for Structural Health Monitoring Applications

Najib Abou Leyla*, Emmanuel Moulin and Jamal Assaad

OAE Department, IEMN, UMR CNRS 8520, University of Valenciennes and Hainaut Cambrésis, 59313 Valenciennes cedex 9, France

Abstract: Many recent studies in different domains exploited the ambient noise correlation to retrieve the Green's function between two points. This technique allows a passive characterization of a given medium in the presence of a perfect diffuse field. The aim of this paper is to apply this principle in an aeronautic context. Thus we are looking to exploit the mechanical vibrations in a plane during the flight, to realize a passive structural health monitoring. Indeed, a natural acoustic noise field is produced by engines and aero acoustic effects. That being said, such a field is not spatially and temporally perfectly diffused, which yields to imperfect conditions where convergence towards the Green's function is not ensured. Despite that, in this paper we show that since the obtained information is sensible to the medium state, it is still exploitable for damage detection. In fact, experimental studies presented in this paper allow verifying two necessary conditions to the applicability of this technique: the reproducibility of the cross-correlation function, and its potential to detect a defect in the medium. Finally, the influence of the source position on the cross-correlation function is shown.

Keywords: Structural health monitoring, acoustic noise correlation.

1. INTRODUCTION

For several years, researches have demonstrated the possibility of retrieving information about the nature of a given medium from natural ambient noise. The theory [1-3] predicts that, assuming the presence of a perfect diffuse field, the cross correlation function between the signals recorded simultaneously at two points converges to the Green's function between these two points. Such techniques are relatively well-known in civil engineering [4, 5], seismology [6, 7], underwater acoustics [8, 9] and ultrasonics [10, 11]. More recently, application to Structural Health Monitoring (SHM) of aeronautical structures has been studied. Sabra *et al.* [12] aimed to exploit the turbulent air-flow around a structure, making the assumption that it generates an almost spatially-diffuse and temporally-random acoustic field in the structure, after a certain period of time. In another study [13], an ultrasonic propagation imaging technology using a scanning pulsed laser and a fixed piezoelectric transducer for damage detection has been developed. In these conditions, the general features of the Green's function could effectively be retrieved and damage detection is demonstrated.

The aim of the work presented here is to apply such techniques in more general conditions. In the particular situation of aeronautic structure, the engines of a plane and the aero acoustic phenomena produce a natural acoustic field. The advantages of such a passive technique, in comparison with classical SHM methods [14, 15], are a reduction of embedded electronics in its physical aspect and reduction of energy consumption. It becomes then realistic to consider autonomous network sensors designed to realize an integrated passive SHM system.

The complexity of this application is the fact that the acoustic field we are looking to exploit is a non-diffuse field because the natural sources are localized, and it presents non-stationary characteristics. Nevertheless, the applicability of this technique is showed in this paper. Indeed, even if the correlation function does not converge to the exact Green's function, it is still exploitable for damage detection because it verifies two important conditions: first, it is reproducible for a given source configuration and second it contains a sufficiently large number of multiple paths to cover virtually all the structure. These two conditions are sufficient for the particular situation where the source position is unchanged. However, the cross-correlation function is sensitive to any source change, which can be misinterpreted as the occurrence of a defect. To overcome this limitation of the application, a solution based on indexing the information contained in the cross-correlation function on the source position has been proposed in a previous work [16]. This paper being dedicated to verify the applicability of the technique, the second section is a simplistic theoretic illustration of the method. The third section is devoted to a numerical study that highlights the influence of a defect on the auto correlation and cross correlation functions. The section 4 is dedicated to confirm experimentally the numerical results and to validate the reproducibility condition, the sensitivity of the cross-correlation function to a defect, and the study of the dependence of the cross-correlation function to the source position. Finally, to overcome the problem caused by the influence of the source position on the cross-correlation function, a solution based

*Address correspondence to this author at the OAE Department, IEMN, UMR CNRS 8520, University of Valenciennes and Hainaut Cambrésis, 59313 Valenciennes cedex 9, France; Tel : + 33 327 51 13 67;
Fax : + 33 327 51 11 89; E-mail: najib.abouleyla@gmail.com

1874-8376/12

on the use of a third receiver is presented and experimentally validated.

2. BACKGROUND AND PRINCIPLE

Let us assume a localized point source *O* emitting an acoustic stationary random signal *e(t)* (Fig. **1**).

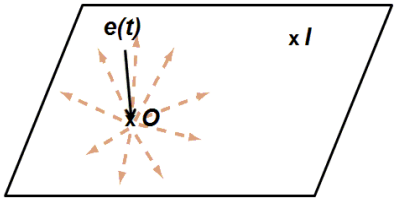

Fig. (1). Theoretical illustration.

The received signal $u_I(t)$ at a point *I* of the structure can then be written as:

$$u_I(t) = g_{OI}(t) \otimes e(t), \quad (1)$$

where $g_{OI}(t)$ is the Time Domain Green's Function (TDGF) between *O* and *I*, and the symbol $\otimes$ is the convolution. Thus, the cross-correlation between two signals received simultaneously at two different points *A* and *B* is given by:

$$\begin{aligned} R_{AB}(t) &= u_A(-t) \otimes u_B(t) \\ &= g_{OA}(-t) \otimes g_{OB}(t) \otimes R_{ee}(t), \end{aligned} \quad (2)$$

with $R_{ee}(t)$ the auto-correlation function of the emitted signal *e(t)*. Consequently, the cross-correlation function depends on the Green's functions between the point source and the receivers, and the emitted signal *e(t)*.

In the frequency domain, equation (2) becomes:

$$\Re_{AB}(\omega) = G^*_{OA}(\omega) G_{OB}(\omega) |E(\omega)|^2, \quad (3)$$

with $\Re_{AB}, G_{OA}, G_{OB}$ are respectively the Fourier-Transforms of R_{AB}, g_{OA}, g_{OB}, $|E|^2$ the module of the Fourier-Transform of the signal *e(t)*, and * the complex conjugate. Thus, in a narrow-frequency band, supposing the amplitude of the spectral-density of the signal constant, the emitted signal will not induce phase-shifting in the cross-correlation function. Therefore, the influence of the spectral density of the source can be easily eliminated.

Notating $g'_{OI}(t)$ the TDGF when a defect appears somewhere in the structure, and $g_{O_kI}(t)$ the TDGF when the source is located at a point O_k. In these two cases (Fig. **2**), the cross-correlation function can be written:

$$R'_{AB}(t) = R_{AB}(t) + \Delta R_{AB}(t) \quad (4)$$

where $\Delta R_{AB}(t)$ depends on $g'_{OI}(t)$ and $g_{O_kI}(t)$, and represents the variation induced by one of the above situations, on the cross-correlation function.

In a general case, where a defect appears in the structure, and the source is located at a given position O_k, $R'_{AB}(t)$ can be written as:

$$R'_{AB}(t) = g'_{O_kA}(-t) \otimes g'_{O_kB}(t) \otimes R_{ee}(t) \quad (5)$$

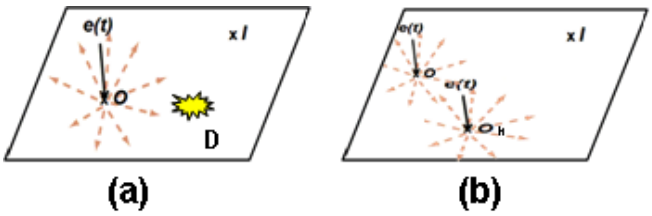

Fig. (2). Green's functions variations. (**a**) Appearance of a defect D, (**b**) Source-position variation.

The principle of the damage detection technique requires the ability to separate between the variations caused by the appearance of a defect (the Green's function changes from $g_{OI}(t)$ to $g'_{OI}(t)$) and those caused by the influence of the source position (difference between the Green's function $g_{OI}(t)$ for a source localized at a point *O*, and the Green's function $g_{O_kI}(t)$ for a source localized at a point O_k).

In the following, a numerical study illustrating the influence of a defect on the applicability of the method in real conditions is presented. The reproducibility of the cross-correlation function, its potential to detect a defect, and its sensitivity to the source characteristics are then demonstrated experimentally. In fact, since the measured cross-correlation is used to monitor the integrity of the structure, it should be reproducible for different measurements done in the same conditions. A second necessary condition to the study is the ability to detect any form of heterogeneity in the structure, using the cross-correlation of the ambient acoustic field. Finally, since the source-position influences the result, it is crucial to avoid misinterpretations by separating changes caused by source motion from those caused by defect appearance.

3. NUMERICAL STUDY

In this section, a modeling tool is developed to estimate the displacement field at a given point *I* for an acoustic stationary random signal emitted at a point *O*. The benefits of such a tool are the possibility to modify some physical parameters such as the reverberation time and other structural properties in order to understand their influence on the final result. After the partial validation of this tool by comparing the results with those obtained by Finite Element Method (FEM) simulation, this tool will be exploited to study the influence of a defect on the auto-correlation and the cross-correlation functions.

3.1. Displacement Field Modeling

The equation (1) can be written in the frequency domain as:

$$U_I(\omega) = G_{OI}(\omega) E(\omega) \quad (6)$$

with $E(\omega)$ the Fourier transform of the emitted signal *e(t)*. In two dimensional study, the Green function is given by:

$$G_{OI}(\omega) = \frac{A(\omega)}{\sqrt{r_{OI}}} \exp\left[-ikr_{OI}\right], \quad (7)$$

with r_{OI} the distance between the source *O* and the receiver *I*, and $A(\omega)$ a function that depends on the plate properties, the type of excitation and the frequency. For far field application $A(\omega)$ is given by [22]:

$$A(\omega) = \frac{(1+i)\omega}{8\sqrt{\pi P_{mm}}} \sqrt{k} \left| u_{mz} \right|^2 , \quad (8)$$

with u_{mz} the modal displacement field of the mode *m* and P_{mm} the pointing vector.

Taking into account the multiple reflections on the edges of the plate, the displacement field at the receiver point *I* is the sum of all the signals received by the image sources. Supposing a total number of N image sources, the displacement field is then given by:

$$U_I(\omega) = \sum_{J=1}^{N} U_{JI}(\omega) = \sum_{J=1}^{N} \frac{A(\omega)}{\sqrt{r_{JI}}} \exp\left[-ikr_{JI}\right], \quad (9)$$

with r_{JI} the distance between the image source *J* and the receiver *I*.

Thus, the cross-correlation between two signals received simultaneously at two different points *A* and *B* is given by:

$$R_{AB}(t) = \int_{-\infty}^{+\infty} \Re_{AB}(\omega) \exp\left[i\omega t\right] d\omega , \quad (10)$$

with $\Re_{AB}(\omega)$ given by:

$$\Re_{AB}(\omega) = U_A^*(\omega) U_B(\omega), \quad (11)$$

with U_A and U_B respectively the displacement fields at two points *A* and *B* computed by the equation 9, and * the complex conjugate.

3.2. Validation of the Modeling Tool by FEM

A plate of dimensions 2m*1m*3mm, a point source *S* located at X_S=1.5m and Y_S=0.75m and a receiver *I* located at X_I=1m and Y_I=0.5m are considered. A pulse is then emitted at the source and a signal of 0.5 seconds is recorded at *I*. The signal is then filtered with a Hanning window of 5 cycles centered at the frequency of 10 kHz. The comparison of the results obtained using the modeling tool and the FEM simulation is shown at the Fig. (**3**).

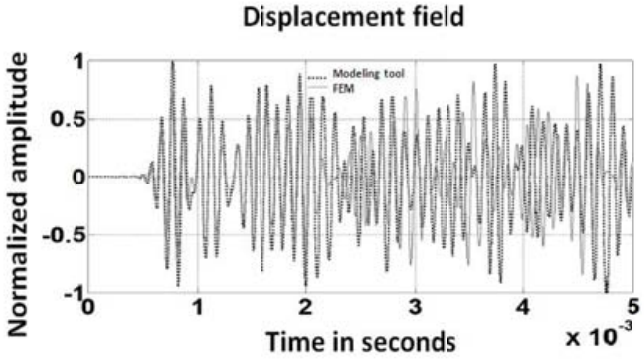

Fig. (3). Displacement field obtained with the modeling tool and the MEF.

We can see that both results fit reasonably well, even though the treatment of the reflection at the plate boundaries is approximated. This results in an unperfect reproduction of the wavepackets shapes, which is not a fundamental aspect in this study. Despite this, the simplified model is much more adapted for the present study than a FEM modeling. Indeed it is much quicker, more compliant (in the sense that the pertinent physical parameters are more directly accessible) and provides better understanding of the physical phenomena involved. Thus, the modeling tool can be conveniently exploited to study the influence of the defect on the auto and cross-correlation functions.

3.3. Influence of the Defect on the Auto-Correlation and Cross-Correlation Functions

A plate of aluminum of dimensions 2m*1m*3mm is considered with two measurement receivers A and B, a reference receiver C and a source S located respectively at the positions X_A=1.2 m, Y_A=0.4 m; X_B=1.4 m, Y_B=0.5 m; X_C=0.25 m, Y_C=0.15 m; and X_S=0.2 m, Y_S=0.1 m. A circular defect of radius 50 mm (Fig. **4**) is modelized through an attenuation of the wavepackets crossing through it and the auto-correlation at *C* and the cross-correlation between *A* and *B* functions are computed with and without the defect, and compared to emphasize the influence of the defect (Fig. **5**).

The comparison between the images of the functions with and without defect shows clearly the influence of the defect. We can see that the defect is clearly detectable using the cross-correlation function, and that, in the configuration tested here, it has much more influence on the cross-correlation function then on the auto-correlation function.

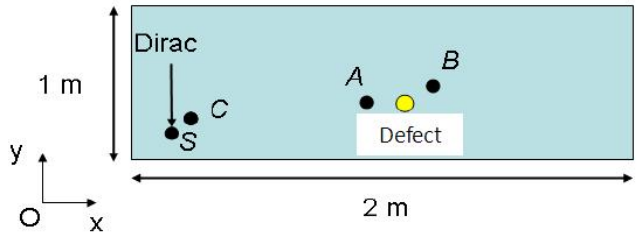

Fig. (4). Source, defect and receivers positions.

Thanks to the numerical modeling tool, it appears thus possible to select suitable receiver positions that, for given plate properties, induce at the same time a low sensitivity of the auto-correlation and a high sensitivity of the cross-correlation to a defect. Besides, complementary numerical results obtained from the same model have shown the strong dependence of the auto-correlation on the source position. All this suggests that it might be possible to overcome the problem of the mixed source and defect effects, by the conjugated use of the auto- and cross-correlation functions.

These interesting phenomena highlighted by the numerical results will be validated experimentally in the next section and then the practical application of the detection method will be more precisely described in Sec. 5.

4. EXPERIMENTAL RESULTS

This section shows the experimental validation of the reproducibility of the cross-correlation function, its

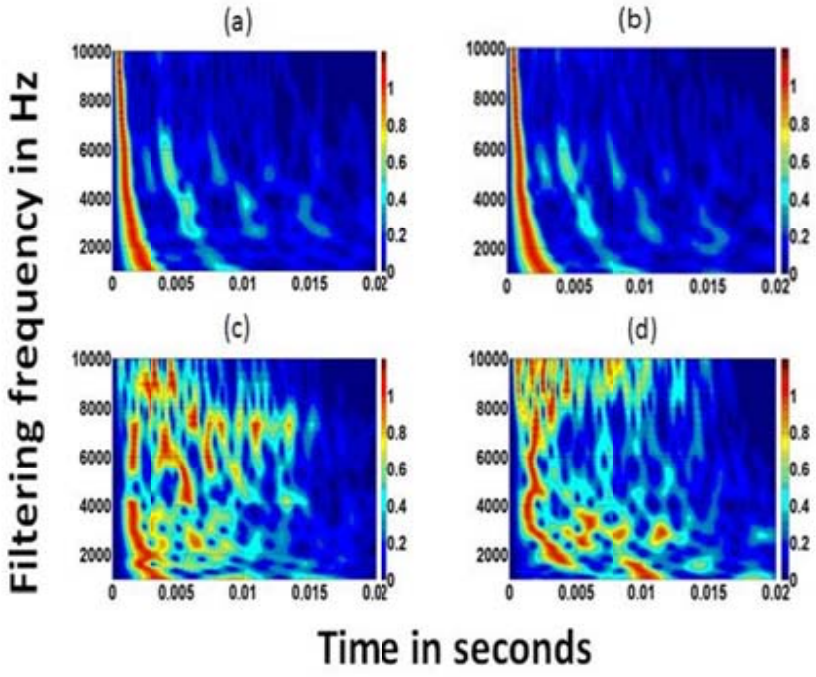

Fig. (5). The auto-correlation function at C (**a**) without and (**b**) with defect, and the cross-correlation function between A and B (**c**) without and (**d**) with defect.

sensitivity to a defect, and highlights the influence of the source position on the final result.

4.1. Reproducibility

To study the applicability of the ambient noise correlation method, experimentation in the laboratory has been set-up in order to verify the reproducibility and the sensitivity of the correlation function to a defect. Thus, an aluminum plate of 2*1 m^2-surface and 6mm-thickness has been considered, and two circle PZ27-piezoelectric transducers of 0.5cm-radius and 1mm-thickness have been glued with honey at two positions *A* and *B*. To generate the ambient acoustic noise in the plate, an electrical noise generator has been used, and the signal has been emitted using a circle PZ27-piezoelectric transducer of 1cm-radius and 1mm-thickness, placed at a position *O*. The signals received at *A* and *B* have been measured and sent to a computer using a GPIB bus (Fig. **6**).

Since the measured time-signal *T* is finite, the expected value of the cross-correlation function (Eq. 2) cannot be exactly computed and should be estimated by a statistical averaging on a finite-time correlation.

An experimental estimation of $R_{AB}(t)$ is then obtained by averaging on *N* acquisitions the following finite-time correlation $C_{AB}(t)$:

$$C_{AB}(t) = \int_0^T u_A(\tau) u_B(t+\tau) d\tau \qquad (12)$$

The Signal-to-Noise-Ratio (SNR) can be increased by augmenting the time measurement *T* and/or the number of averages *N* [17]. That said, from the moment when *T* is longer than the ring time T_r (or reverberation time) of the structure, nothing will be gained by augmenting *T*.

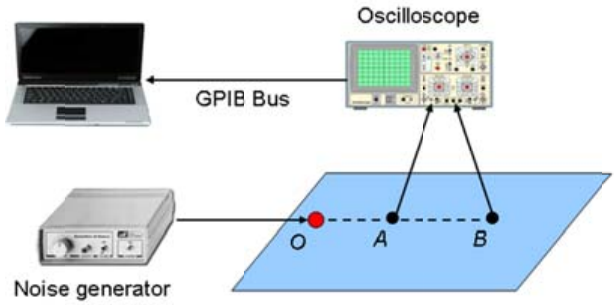

Fig. (6). Experimental set-up for studying reproducibility.

The ring time of the structure being estimated to T_r = 100 ms [16], a signal-length of *T* = 500 ms has been considered.

The cross-correlation between these two signals has then been computed and averaged on *N* = 150 acquisitions to increase the signal-to-noise ratio.

Finally, in order to better analyze the signals, a time-frequency representation has been used. Thus, a wavelet-transform of the measured cross-correlation function has been computed by convolving with a 5-cycle Hanning-windowed sinusoid of variable central frequency f_0. A summary of the signal processing done for experimental results is shown at Fig. (**7**).

A time-frequency representation of the cross-correlation function, in the frequency-band [1-6 kHz], is shown at Fig. (**8**). We localize some zones (circled zones), where the amplitude is very low, that characterize the source position in the structure.

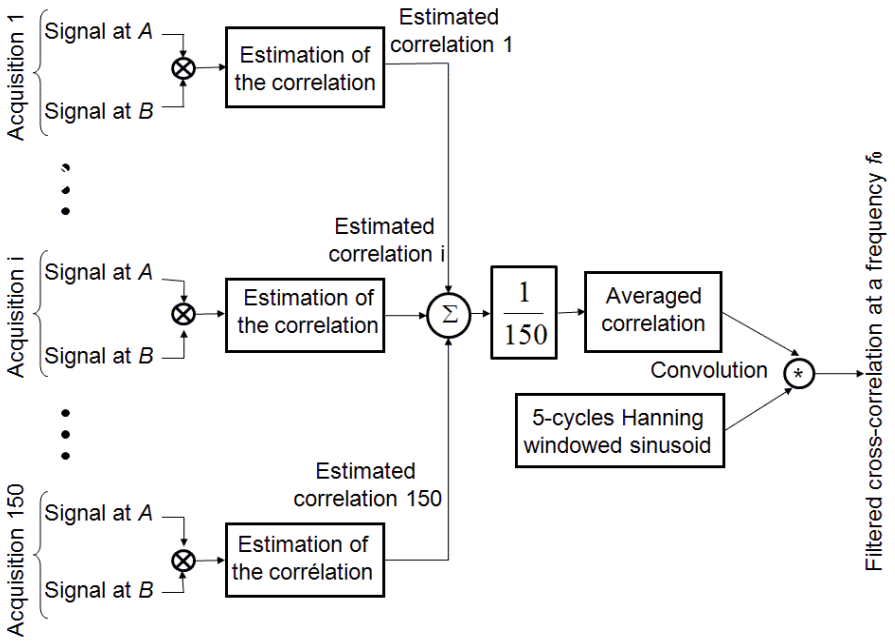

Fig. (7). Signal processing for measurements.

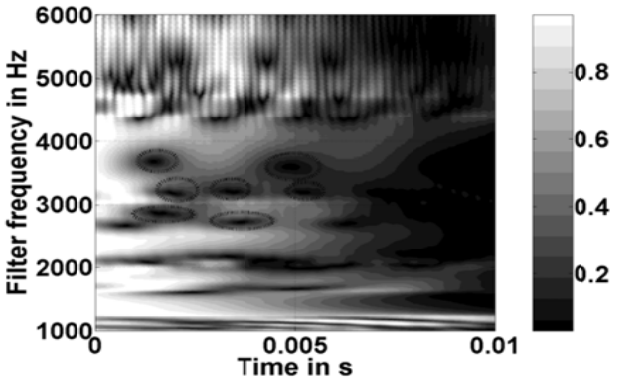

Fig. (8). Time-Frequency representation of the cross-correlation function.

In fact, the source-position to the structure-geometry makes local destructive contributions of the signals (direct and reflections). This parameter will be exploited later in this paper (section 4) to classify the source characteristics using image processing.

In the following, for a clear demonstration of the measurements, results will be shown for a single frequency of filtering.

Repeating the measurements for a given source configuration, we obtain a reproducible cross-correlation function for a large band of frequencies starting at 2 kHz and up to 100 kHz (Fig. **9**).

The curves of the filtered average cross-correlation functions presented in Fig. (**6**), show that for almost all frequencies, the correlation is reproducible for a given source configuration. That said, the reproducibility is less clear for

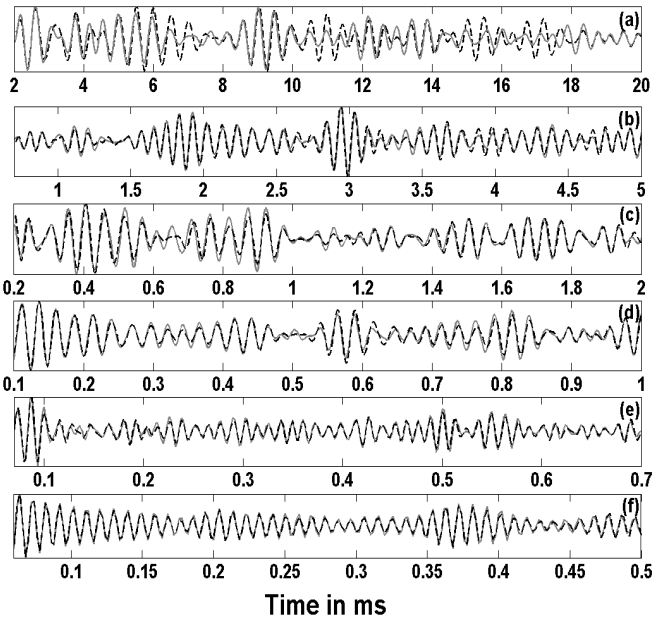

Fig. (9). Normalized-filtered-averaged cross-correlation functions for the 1st measurement (broken line) and the 2nd measurement (solid line). (**a**) f_0 = 2 kHz, (**b**) f_0 = 10 kHz, (**c**) f_0 = 20 kHz, (**d**) f_0 = 40 kHz, (**e**) f_0 = 70 kHz, (**f**) f_0 = 100 kHz.

2 kHz than for frequencies above 10 kHz. This can be explained by the fact that the SNR for high frequencies is higher than the SNR ratio for low frequencies, for the transducers used in this experimentation.

The reproducibility for low frequencies can be improved by increasing the number of averages. In fact, since high frequencies are dominant with the used transducers, an average on 150 acquisitions seemed to be enough on the temporal signal without filtering to converge to a reproducible cross-correlation function.

4.2. Sensitivity to a Defect

In this section, the sensitivity of the cross-correlation function to a defect is studied. Thus, two measurements have been done, one without a defect and the other with a defect somewhere in the plate (Fig. **10**).

Concerning the modeling of the defect, for repeatability purpose, an aluminum disk of 1 cm-radius has been glued on the surface of the plate between the two points *A* and *B*.

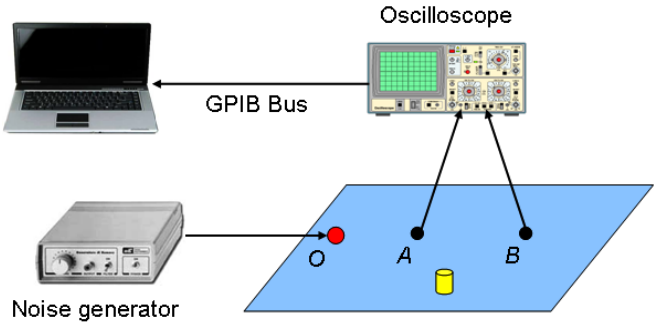

Fig. (10). Experimental set-up for defect detection.

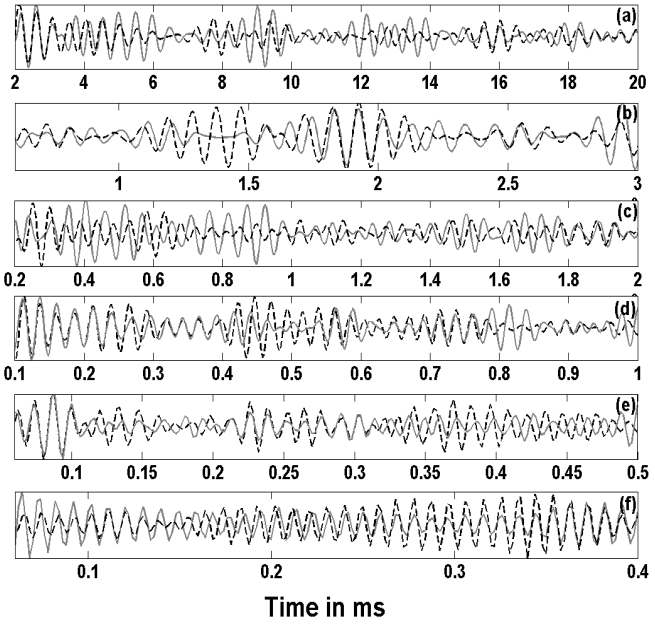

Fig. (11). Normalized-filtered-averaged cross-correlation functions with (broken line) and without defect (solid line). (**a**) f_0 = 2 kHz, (**b**) f_0 = 10 kHz, (**c**) f_0 = 20 kHz, (**d**) f_0=40 kHz, (**e**) f_0 = 70 kHz, (**f**) f_0 = 100 kHz.

In fact, such a defect introduces local heterogeneity from an acoustic impedance change point of view.

The filtered-averaged cross-correlation functions shown at Fig. (**11**) highlight the sensitivity of the cross-correlation function to a defect, for a large band of frequencies.

In fact, the comparison of the cross-correlation function without the presence of a defect (solid line) and with defect (broken line), reveals an amplitude variation and a phase-shifting introduced by the appearance of the defect, which is typically similar to an active pitch-catch measurement result [18].

4.3. Influence of the Source Characteristics

The reproducibility and the sensitivity to a defect of the cross-correlation function being verified, this section will deal with the study of the influence of the source position on the correlation function. To better highlight the influence of the source position on the cross-correlation function, experimentation with three source positions is shown. A first one (O_1 aligned with the points *A* and *B*, a second one (O_2) off-centered from the direction [*A*-*B*], and a third one (O_3) more skewed (Fig. **12**).

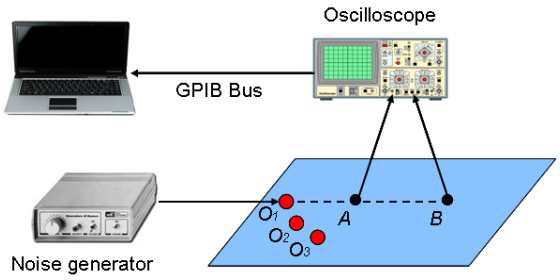

Fig. (12). Influence of the source position.

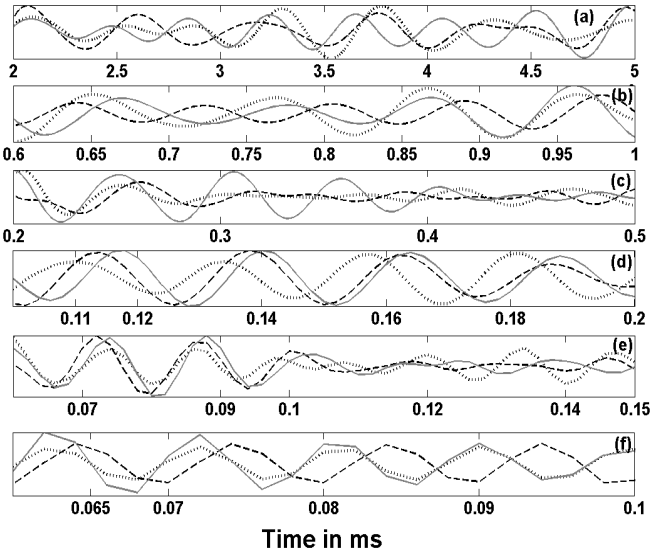

Fig. (13). Normalized-filtered average cross-correlation functions for S1 (solid line), S2 (broken line), and S3 (dashed line). (**a**) f_0 = 2 kHz, (**b**) f_0 = 10 kHz, (**c**) f_0 = 20 kHz, (**d**) f_0 = 40 kHz, (**e**) f_0 = 70 kHz, (**f**) f_0 = 100 kHz.

The curves of the filtered-averaged cross-correlation functions presented at Fig. (**13**) for the three source positions show a clear source position dependence of the cross-correlation function, with amplitude variations and phase shifts. However, the observed phase shifts are not representative of the variation of the source, and are not easily linked to the source position. In fact, the considered medium is very reverberant, and the waves are only lightly attenuated and propagated on long distances. Thus, the received signals at the points *A* and *B* come from a large number of reflections and multi-paths, and are overlapped in an unpredictable manner. The cross-correlation function is thus clearly dependent of the source position.

5. PRACTICAL APPLICATION OF THE METHOD

The position of the source is inseparable parameter in the information contained in the cross-correlation function between the measurement receivers *A* and *B*. A solution to this problem, as suggested by the numerical results of Sec. 3, is to introduce a third transducer *C* [16], called "reference transducer", and used to identify the source position as a first step of the medium inspection (Fig. **14**). This solution is inspired by the impact localization application based on one-channel time reversal [19].

A database containing the auto-correlations at *C,* and the cross-correlations between *A* and *B* of all the possible source positions for a healthy plate (without defect), has been created.

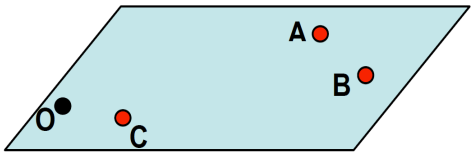

Fig. (14). Experimental configuration.

Using the same notation as in section 2, the estimated auto-correlation at *C*, for a given source position O_k can be written:

$$R_{O_kC}(t) = u_C(-t) \otimes u_C(t) = g_{O_kC}(-t) \otimes g_{O_kC}(t) \otimes R_{ee}(t), \quad (13)$$

and the estimated cross-correlation between *A* and *B* for a given source position O_k can be written as:

$$R^k_{AB}(t) = u_A(-t) \otimes u_B(t) = g_{O_kA}(-t) \otimes g_{O_kB}(t) \otimes R_{ee}(t). \quad (14)$$

As mentioned in section 3, the estimations (Eq. 6) of $R_{O_kC}(t)$ and $R^k_{AB}(t)$ will be noted respectively $C_{O_kC}(t)$ and $C^k_{AB}(t)$.

The proposed solution consists of two steps. In the first step, the source position is identified by comparing the measured auto-correlation on the reference receiver with all the auto-correlations of the database. The most similar one is then chosen. Supposing the total number of the source configurations equal to *M,* Fig. (**15**) schematizes the identification of the source configuration.

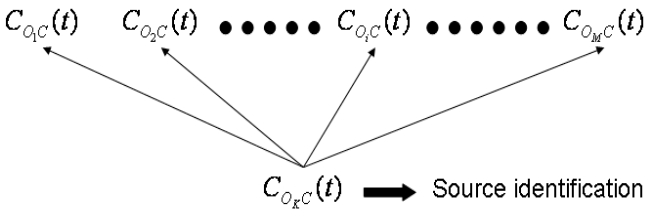

Fig. (15). Source identification.

The second step consists of comparing the measured cross-correlation to the cross-correlation of the identified source configuration for a healthy plate. The differences between these two cross-correlations reflect the effect of the defect. The schema of the Fig. (**16**) summarizes the different stages of the proposed solution.

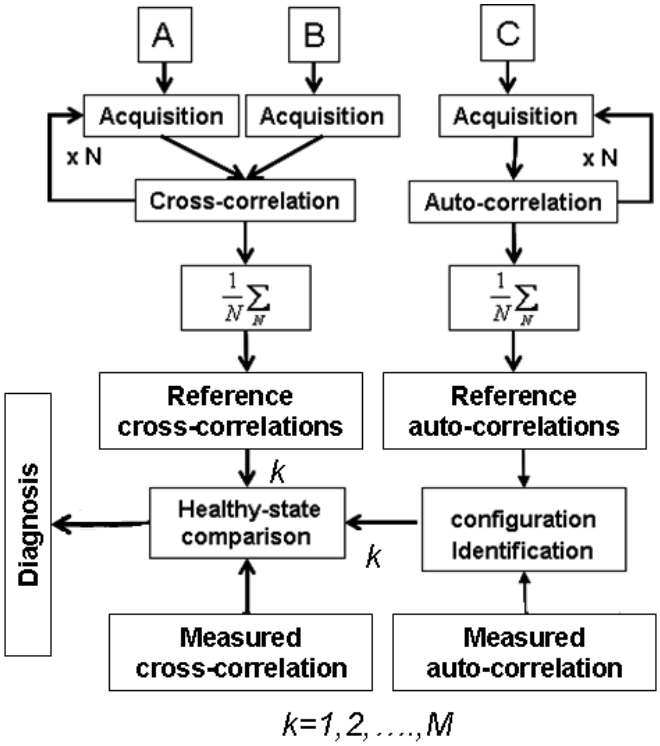

Fig. (16). Principle of the proposed solution.

To validate experimentally this solution, measurements for two source positions S_1 and S_2 are shown. The cross-correlations between *A* and *B*, and the auto-correlations at *C* for a healthy plate have been saved in a database.

A defect has then been introduced, and the cross-correlation between *A* and *B*, and the auto-correlation at *C* have been measured. The measured auto-correlation is compared to the two auto-correlations of the healthy-state (Fig. **17**). This comparison allows identifying the source position, which is the first one in this case.

In the second step, the cross-correlation of the first source configuration is compared to the measured cross-correlation (Fig. **18**).

The comparison between the two images of Fig. (**18**) shows differences induced by the appearance of defect somewhere into the plate, since the influence of the source configuration was eliminated in the first step of the source position identification. In the same time, though, it can be remarked that clear similarities still exist in both images. This can be explained by the fact that the correlation reflects the modification of the repartition of some (and not all the) wave packets in the signals due to the presence of a defect. Only the waves that meet the defect on their paths are modified. The important point, however, is that some modifications are indeed detectable, which enables the detection of the defect. These differences are highlighted by the circled zones in Fig. (**18**). Note that time representations at conveniently selected frequencies would make the differences more visible for the human observer (but not for an algorithm!), as already illustrated in Sec. 4 (see Fig. **11**).

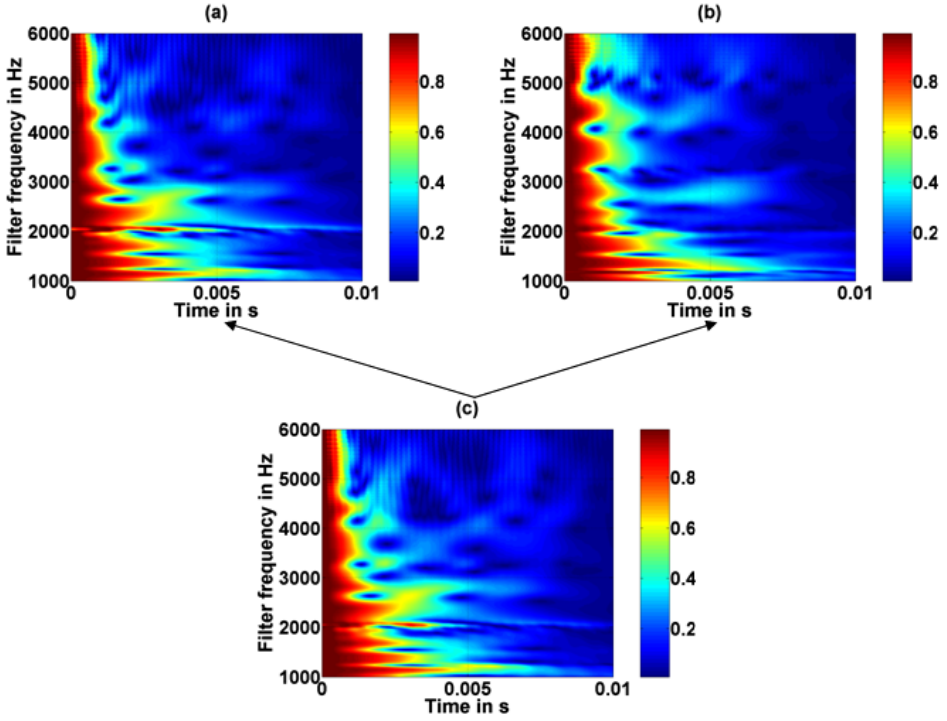

Fig. (17). Source position identification. Healthy-plate auto-correlations for the source position number (**a**) No.1 (**b**) No. 2, (**c**) measured cross-correlation with defect.

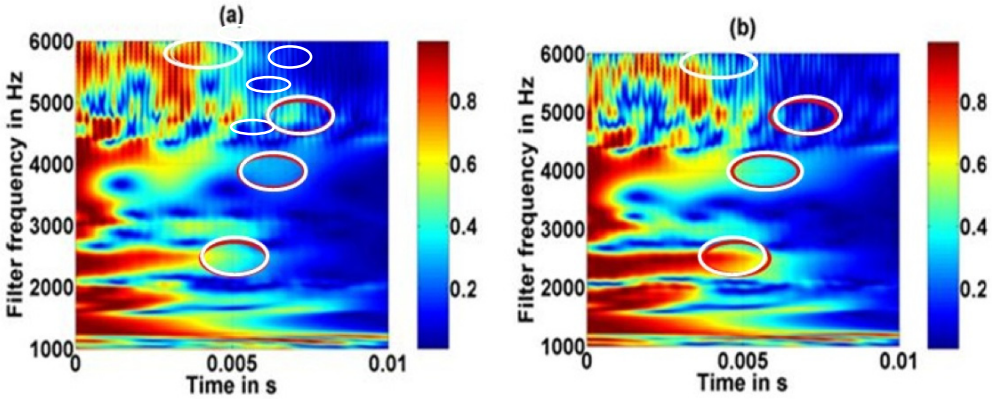

Fig. (18). Defect detection. Cross-correlations for the same source configuration. (**a**) without defect, (**b**) with defect.

For experimental validation of the proposed solution, an illustration with two source positions is enough, but for a real application with a large number of source positions, an image processing algorithm based on the mean square error can be used to identify with a high precision the source position. In fact different metrics such as PSNR (Peak Signal-to-Noise Ratio) [20], and more recently the SSIM (Structural SIMiliraty) [21] allow to measure the similarity between two images.

These encouraging results pushed us to elaborate a sophisticated theoretic study to optimize the proposed solution. Thus, a quantification of the sensitivity of the cross-correlation function between the measurement sensors *A* and *B*, and the auto-correlation at the reference sensor, to a defect has been done. This quantification is based on the relative positions of the noise source, the sensors, and the defect. The results of this study are under progress.

6. CONCLUSION

In this paper, the applicability of acoustic noise correlation to structural health monitoring in aeronautic context is presented. A modeling tool is developed to estimate the auto-correlation and cross-correlation functions. This tool is validated with comparison to FEM results, and exploited to study the detectability and the influence of the defect on the auto-correlation and cross-correlation functions. The second part of this paper is dedicated to verify experimentally the potential of this technique for SHM applications. Thus, two essential conditions: the reproducibility of the cross-correlation function and its potential in detecting a defect are experimentally validated. The problem caused by the influence of the source position is also studied, and a solution based on using a third transducer to avoid false interpretation of the measurements is presented and a complete description of the measurement

process is proposed. The results obtained numerically and experimentally are coherent.

ACKNOWLEDGEMENTS

None declared.

CONFLICT OF INTEREST

None declared.

REFERENCES

[1] Lobkis OI, Weaver RL. On the emergence of the Green's function in the correlations of a diffuse field. J Acoust Soc Am 2001; 110: 3011-7.

[2] Derode P, Larose E, Tanter M, *et al*. Recovering the Green's function from field-field correlations in an open scattering medium (L). J Acoust Soc Am 2003; 113: 2973-6.

[3] Roux P, Kuperman WA, The NPAL Group. Extracting coherent wavefronts from acoustic ambient noise in the ocean. J Acoust Soc Am 2004; 116: 1995-2003.

[4] Farrar C, James G. System identification from ambient vibration measurements on a bridge. J Sound Vib 1997; 205: 1-18.

[5] Nagayama T, Abe M, Fujino Y, Ikeda K. Structural identification of a non-proportionally damped system and its application to a full-scale suspension bridge. J Struct Eng 2005; 131: 1536-40.

[6] Snieder R, Sheiman J, Calvert R. Equivalence of the virtual source method and wave field deconvolution in seismic interferometry. Phys Rev 2006; 73: 066620.

[7] Shapiro NM, Campillo M, Stehly L, Ritzwoller M. Highresolution surface-wave tomography from ambient seismic noise. Science 2005; 29: 1615-7.

[8] Sabra KG, Dowling DR. Blind deconvolution in ocean waveguides using artificial time reversal. J Acoust Soc Am 2004; 116: 262-71.

[9] Roux P, Kuperman WA, The NPAL Group. Extracting coherent wavefronts from acoustic ambient noise in the ocean. J Acoust Soc Am 2004; 116, 1995-2003.

[10] Larose E, Lobkis OI, Weaver RL. Passive correlation imaging of a buried scatterer (L). J Acoust Soc Am 2006; 6: 119.

[11] Snieder R. Extracting the green's function from the correlation of coda waves: A derivation based on stationnary phase. Phys Rev 2004; 69: 46610.

[12] Sabra KG, Winkel ES, Bourgoyne DA, *et al*. Using cross correlations of turbulent fow-induced ambient vibrations to estimate the structural impluse response. Application to structural health monitoring. J Acoust Soc Am 2007; 4: 121.

[13] Jung-Ryul L, Takatsubo J, Toyama N, Kang D. Health monitoring of complex curved structures using an ultrasonic wavefield propagation imaging system. Meas Sci Technol 2007; 18: 3816.

[14] El Youbi F, Grondel S, Assaad J. Signal processing for damage detection using two different array transducers. Ultrasonics 2004; 42: 803-6.

[15] Grondel S, Assaad J, El Youbi F, Moulin E, Abou Leyla N. Experimental Lamb mode identification in a plate containing a hole using dual signal processing. Meas Sci Technol 2006; 19: 125703.

[16] Moulin E, Abou Leyla N, Assaad J, Grondel S. Applicability of acoustic noise correlation to structural health monitoring in non-diffuse field conditions. Appl Phys Lett 2009; 95: 094104.

[17] Lobkis OI, WeaverRL. On the emergence of the Green's function in the correlations of a diffuse field. J Acoust Soc Am 2001; 110, 3011-7.

[18] Li F, Meng G, Ye L, Lu Y, Kageyama K. Dispersion analysis of Lamb waves and damage detection for aluminum structures using ridge in the time-scale domain. Meas Sci Technol 2009; 20: 95704.

[19] Ing RK, Quieffin N, Catheline S, Fink M. In solid localization of finger impacts using acoustic time-reversal process. Appl Phys Lett 2005; 87: 204104.

[20] Huynh-Thu Q, Ghanbari M. Scope of validity of PSNR in image/video quality assessment. Electron Lett 2008; 44: 800-1.

[21] Wang Z, Bovik AC, Sheikh HR, EP Simoncelli. Image quality assessment: from error visibility to structural similarity. IEEE Trans Image Process 2004; 13: 600-12.

[22] Moulin E, Grondel S, Baouahi M, Assaad J. Pseudo-3D modeling of a surface-bonded Lamb wave source (L). J Acoust Soc Am 2006; 119 (5): 2575-8.

Received: December 25, 2011 Revised: March 13, 2012 Accepted: March 14, 2012